

RECEIVED
JUL 01 1998
QSTI

IN-SITU OBSERVATION OF ATOMIC PROCESSES IN
NANOCRYSTALS EMBEDDED IN Al*

K. Mitsuishi¹, M. Song¹, K. Furuya¹, R. C. Birtcher²,
C. W. Allen², and S. E. Donnelly³

¹National Research Institute for Metals
Sakura, Tsukuba 305, Japan

²Materials Science Division
Argonne National Laboratory
9700 S. Cass Ave.
Argonne, IL 60439

³Department of Physics
University of Salford
Manchester, United Kingdom

February 1998

The submitted manuscript has been created
by the University of Chicago as Operator of
Argonne National Laboratory ("Argonne")
under Contract No. W-31-109-ENG-38 with
the U.S. Department of Energy. The U.S.
Government retains for itself, and others
acting on its behalf, a paid-up, non
exclusive, irrevocable worldwide license in
said article to reproduce, prepare derivative
works, distribute copies to the public, and
perform publicly and display publicly, by or
on behalf of the Government.

Submitted to the Materials Research Society, Boston, MA, December 1-5, 1997.

*Work supported by the U. S. Department of Energy, BES-Materials Sciences,
under Contract W-31-109-Eng-38.

DISCLAIMER

This report was prepared as an account of work sponsored by an agency of the United States Government. Neither the United States Government nor any agency thereof, nor any of their employees, make any warranty, express or implied, or assumes any legal liability or responsibility for the accuracy, completeness, or usefulness of any information, apparatus, product, or process disclosed, or represents that its use would not infringe privately owned rights. Reference herein to any specific commercial product, process, or service by trade name, trademark, manufacturer, or otherwise does not necessarily constitute or imply its endorsement, recommendation, or favoring by the United States Government or any agency thereof. The views and opinions of authors expressed herein do not necessarily state or reflect those of the United States Government or any agency thereof.

DISCLAIMER

**Portions of this document may be illegible
in electronic image products. Images are
produced from the best available original
document.**

IN-SITU OBSERVATION OF ATOMIC PROCESSES IN Xe NANOCRYSTALS EMBEDDED IN Al

K. Mitsuishi, M. Song, K. Furuya *, R. C. Birtcher, C. W. Allen **, and S. E. Donnelly †

* National Research Institute for Metals, Sakura, Tsukuba 305, Japan

** Materials Science Division, Argonne National Laboratory, Argonne, IL 60439, USA

† Department of Physics, University of Salford, Manchester, UK

ABSTRACT

Self-organization processes in Xe nanocrystals embedded in Al are observed with in-situ high-resolution electron microscopy. Under electron irradiation, stacking fault type defects are produced in Xe nanocrystals. The defects recover in a layer by layer manner. Detailed analysis of the video reveals that the displacement of Xe atoms in the stacking fault was rather small for the Xe atoms at boundary between Xe and Al, suggesting the possibility of the stacking fault in Xe precipitate originating inside of precipitate, not at the Al/Xe interface.

INTRODUCTION

Recently, nanocrystals have attracted fundamental and applied interest in materials research because various properties such as, electrical, optical, and magnetic properties, largely depend on size and/or shape of the crystals. The behavior of nanometer size precipitates created by implantation of inert gases in materials has been studied extensively for more than 35 years because of problems associated with the development of fusion and fission reactors[1].

When it is implanted at room temperature, the rare gas Xe precipitates as nanocrystals less than 4nm diameter and mesotactically aligned with the surrounding matrix. The lattice parameter of the precipitates varies with the precipitate size and the combination of gas and metal matrix [2, 3, 4]. The shape and topotactical alignment of the precipitates have been established by high-resolution electron microscopy (HRTEM) [5, 6].

However, little is known about the movement of individual atoms, or structural changes at the atomic level that are necessary to know when one tries to understand the self-organization processes. Therefore, the motivation for following the movement of individual atoms in-situ is very strong. Although HRTEM equipped with a video system can be one of the most promising tools for this purpose, there is an obstacle to surmount that the Xe lattice image is overlapped with Al fringes, because the Xe nanocrystals are embedded in the Al matrix. Therefore, in order to extract the Xe image, it is required to perform some sort of image processing such as FFT, which interfere with in-situ observation.

In this paper, we use the specific off-Bragg condition to extract the Xe lattice image in-situ, and observe self-organization process of Xe, such as inducement and recovery of the defect under electron irradiation.

EXPERIMENT

Specimen preparation

The Al specimens were cut from 5-9's starting material and electronically polished using an electrolyte of HNO_3 : $\text{CH}_3\text{OH} = 1:2$ at 253 K and implanted with 30 keV Xe at room temperature to a dose of $3 \times 10^{20} \text{ ions/m}^2$. Specimens were then annealed at 523 K for 0.5 h in a vacuum to remove radiation damage in the Al matrix and to consolidate the Xe within the precipitates.

Templer et al.[7] have reported that such annealing results in sharper precipitate image and more intense electron diffraction from the solid Xe in Al.

HRTEM observation

HRTEM observations were performed with a JEM ARM-1000 high-voltage TEM, operated at a voltage of 1 MV with a spatial resolution of 0.13 nm, with the incident electron beam tilted slightly from a $\langle 110 \rangle_{Al}$ direction. The defocus values were also chosen to realize specific off-Bragg condition to extract the Xe lattice image.

The electron beam current density was $1.3 \times 10^5 \text{ A/m}^2$ to stimulate the system.

Models for simulation

Xe precipitates in an Al lattice were modeled as a tetradecahedron with faces parallel to $\{111\}_{Xe}$ and $\{100\}_{Xe}$ in Al cavities faceted on these crystal planes[8, 9]. The lattice parameter of the FCC Xe crystal was chosen to be 50% larger than that of Al, consistent with electron diffraction data. Relaxation of interface atoms is not included.

Multi-slice image simulations were carried out to simulate images from the JEM ARM-1000 at 1000keV, where the spherical aberration coefficient C_s is 2.6 mm, the spread of defocus δ is 10 nm and the beam semi-divergence α is 0.3 mrad. The defocus value was varied from +28 to -160 nm. Scherzer defocus for structure imaging is about -56 nm.

RESULTS

Off-Bragg condition

Fig.1 shows a HRTEM image of Xe precipitates in Al with the selected area diffraction pattern. The incident electron beam is parallel to $\langle 011 \rangle$. Atoms appear as black dots in this image taken near Scherzer defocus. Two-dimensional Moiré patterns along one $\langle 100 \rangle$ and two $\langle 111 \rangle$ directions are seen. Both the Moiré patterns of HRTEM and the spacing of the diffraction spots in the SAD pattern indicate that the Xe precipitates are FCC and are mesotacitic with the Al matrix with a lattice spacing about 50% larger than that of Al. A similar observation has been reported by Donnelly et al[10].

In fig. 2, the calculated images of Xe precipitate in $[011]$ direction are shown. The simulated image at Scherzer defocus is in qualitative agreement with the HRTEM image in fig.1. As in fig. 1, the shape of the precipitate is not clear although the image itself is very clear, because the Xe lattice image is overlapped with Al matrix lattice fringes. In this case, it is impossible to perform in-situ observation of recovery processes in the Xe.

To extract the Xe precipitate image from that of the Al matrix, a specific off-Bragg condition is used. The diffraction spots of Xe precipitates are spread in reciprocal space while Al matrix spots are more localized, so that the appropriate selection of illumination angle may weaken the Al lattice fringe and strengthen the contrast of Xe precipitate. The optimum defocus value is also determined by the contrast transfer function in effect detuning the Al matrix image in favor of that of the Xe. The resultant image, therefore, is mainly constructed from Xe spots.

Fig.3 shows the HRTEM image obtained by the specific off-Bragg condition that the electron beam direction is illuminated about 3 degree to a $[1\bar{1}1]$ direction from $[011]$ direction, and the defocus value is taken as -76 nm. Al lattice fringes are weak and the Xe precipitate can be observed clearly. It should be noted that the interpretation of such images needs some care because the defocus is not at Scherzer. It is confirmed that the black spots in fig. 3 correspond to the Xe atoms by multi-slice calculations of specific off-Bragg condition [11].

Defect inducement

Fig. 4 is video-captured images of a defect introduced in the Xe precipitate. Fig. 4 (a) shows the frame of immediately before its introduction, and fig. 4 (b) is just afterwards. The white arrows indicate the plane {111} the defect lies on. The defect is parallel to the $\langle 110 \rangle$ projected direction. The first few atomic lines of Xe from the bottom are not displaced, and the mismatch of the Xe line occurred at forth atom row from right side, coming to the gap between third and forth line of left. The displacement of Xe atoms which forms the stacking fault depends on the atom location, and surprisingly, the displacement was rather small for the Xe atoms at boundary between Xe and Al. This suggests the possibility of the defect in the Xe precipitate originating within the precipitate, not from the Al/Xe interface. By the argument of surface energy of Xe precipitates in Al matrix, in general, it is believed that the shape of the Xe precipitates is strongly confined by Al at the interface [12, 13]. However, it is not clear in this instance that the defect is caused by the boundary.

Because the Xe precipitates are FCC, this defect is stacking fault type defect. To confirm this, a simple calculation of stacking fault in a Xe precipitate neglecting again the interface relaxation, was performed. Fig. 5 shows the result of calculation for the defocus value $\Delta = -76$ nm. The calculated image of the defect shape coincides well with the experimental regardless of the shapes of interface. Therefore, the defect can be considered as stacking fault type defect.

Recovery process

The successive recovery of the defect is shown in fig.6 where white arrows indicate the layers of atoms moved and the black arrows indicate the direction of movement. The numbers are the time, measured from the first observation of the defect in seconds. The recovery occurred within a layer unit. Since the time intervals of events in each layer are long, a few seconds, each step of the process is spread over many frames of the video and is visible at normal video recording speed.

In fig. 6 (d), opposite movement of the layer previously recovered is observed, and in fig. 6 (e), several layers recover at the same time. This illustrates the delicate balance of forces involved in the recovery processes.

CONCLUSION

High-resolution transmission electron microscopy (HRTEM) was carried out on Al TEM thinned specimens implanted with 30keV Xe^+ at room temperature to a dose of 3×10^{20} ions/ m^2 . Self-organization processes in Xe nanocrystals embedded in Al were observed with in-situ electron microscopy technique by tilting the electron beam about 3 degree from a $\langle 011 \rangle$ direction and defocusing the objective lens -76 nm. It is revealed that the displacement of Xe atoms which forms the stacking fault was rather small for the Xe atoms at the Xe/Al interfaces.

This may suggests that the stacking fault in the Xe precipitate is originates inside of precipitate for the particular Xe precipitate presented here, but it is difficult to decide only by two dimensional image of HRTEM.

Recovery occurs in a layer by layer manner rather slowly so that the process can be recorded by a standard video system.

REFERENCES

1. V. N. Chernikov, W. Kesternich and H. Ullmaire, J. Nucl. Mater. 227, 157, (1996).
2. R. C. Birtcher and C. Liu, J. Nucl. Mater. 165, 101 (1989).

3. R. C. Birtcher and W. Jäger, Ultramicroscopy 22,267 (1987).
4. R. C. Birtcher, S. E. Donnelly and C. Templier, Phys. Rev. B, 50, 764 (1994).
5. S. E. Donnelly and C. J. Rossouw, Phys. Rev. B13,485 (1986).
6. D. I. Potter and C. J. Rossouw, J. Nucl. Mater. 161, 124 (1989).
7. C. Templier, H. Garem, J. P. Riviere and J. Delafond, Nucl. Instr. and Meth. B18, 24 (1986).
8. L. Gråbæk, J. Bohr, H. H. Andersen, A. Johansen, E. Johnson , L. Sørholt-Kristensen and I. K. Robinson, Phys. Rev. B45, 2628 (1992).
9. S. Q. Xiao, E. Johnson, S. Hindenberger, A. Johannsen, K. K. Bourdelle and U. Dahmen, J. Microscopy 180, 61 (1995).
10. S. E. Donnelly, C. J. Rossouw, and I. J. Wilson, Radiat. Eff. 97, 265 (1986).
11. K. Mitsuishi, M. Song, K. Furuya, R. C. Birtcher, C. W. Allen, and S. E. Donnelly, presented at the 1997 Jpn.Phys.Soc. Meeting, Kobe, Jpn, 1997(unpublished).
12. N. Ishikawa, M. Awaji, K. Furuya, R. C. Birtcher, C. W. Allen, Nucl. Instrum. Methods B127/128, 123 (1997).
13. M. S. Anderson and C. A. Swenson, J. Phys. Chem. Solids 36,145 (1975).

Figure 1: High-Resolution TEM (HRTEM) image of Xe precipitates in Al, observed near Scherzer defocus (a) with selected area diffraction pattern (b). The incident electron beam is parallel to $\langle 011 \rangle$.

Figure 2: The results of multi-slice image simulations of a Xe precipitate in Al matrix at different defoci (Df) with [011] direction. a) Df = 0 nm, b) Df = -45 nm, c) Df = -55 nm (Scherzer defocus), d) Df = -65 nm, e) Df = -100 nm and f) Df = -165 nm.

Figure 3: HRTEM image obtained in an off-Bragg condition. The electron beam direction is tilted about 3 degree toward a $[1\bar{1}1]$ from [011] zone axis, and the defocus value is taken as -76 nm. Al lattice fringes are weak and Xe precipitate can be observed clearly.

Figure 4: Video captured images of the defect introduction in a Xe precipitate; (a) immediately before the event, (b) immediately afterward. The white arrows indicate the plane of the defect.

Figure 5: Simulated image of the stacking fault type defect induced in Xe nanocrystal. The defect is in $\{111\}$.

Figure 6: The successive images of the defect recovery. The white arrow indicates the layer in which the recovery occurred, and the black arrow indicates the direction of movement. The number indicates the time in seconds, measured from the first observation of the defect.

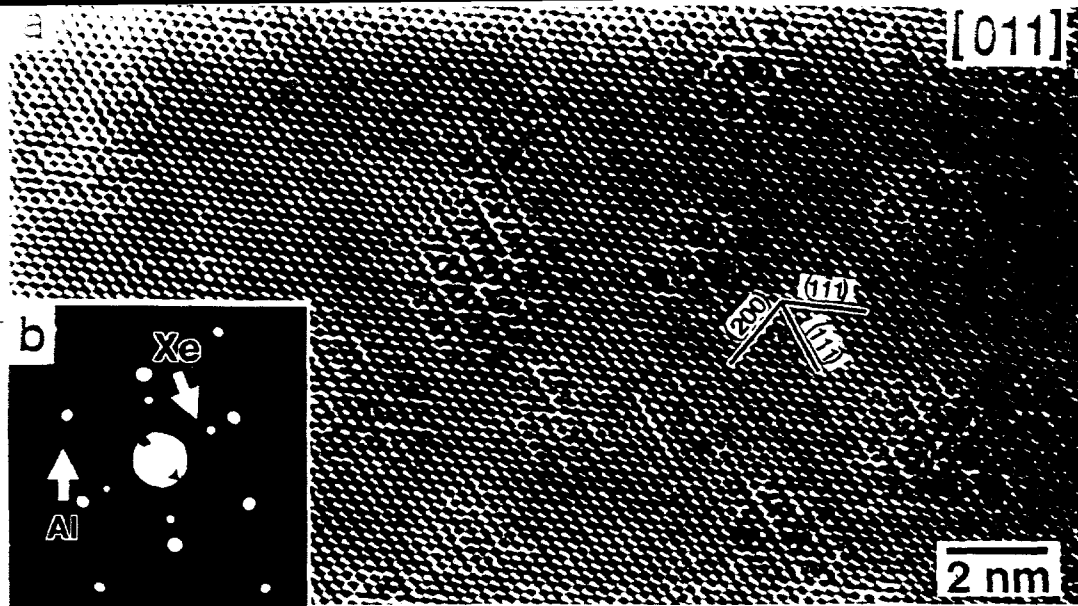


Figure 1.

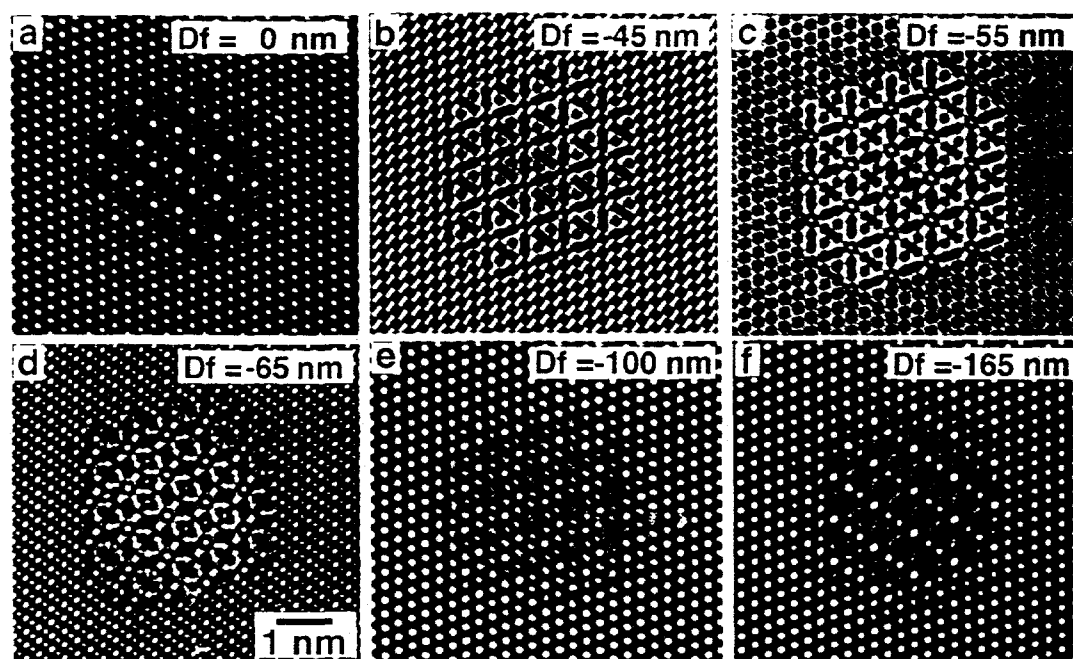


Figure 2.

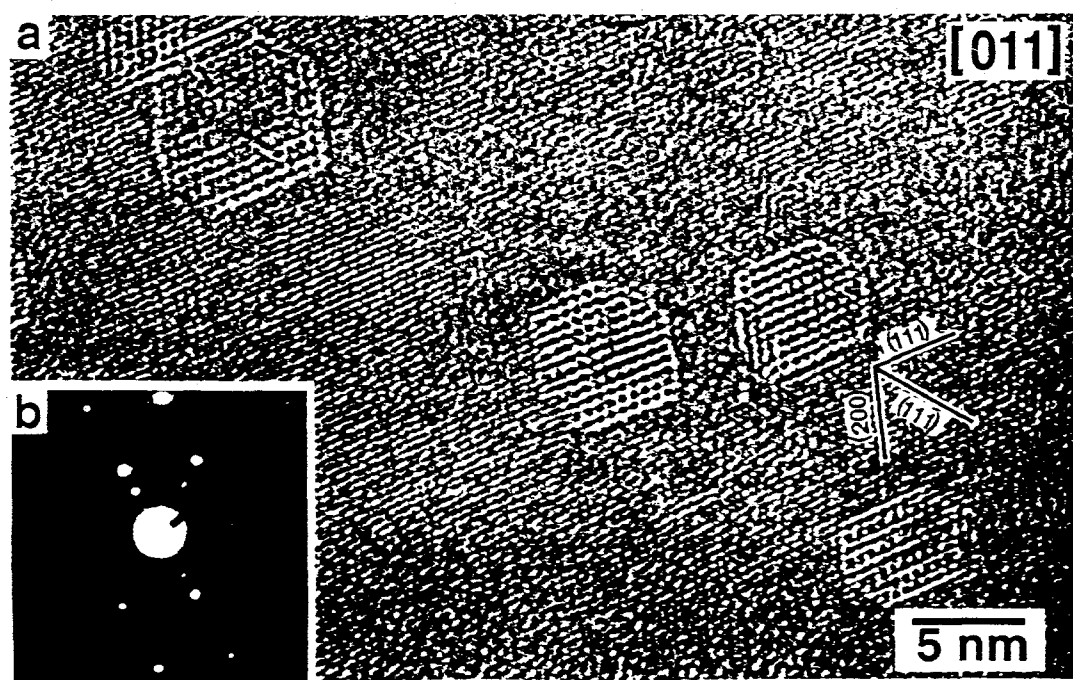


Figure 3.

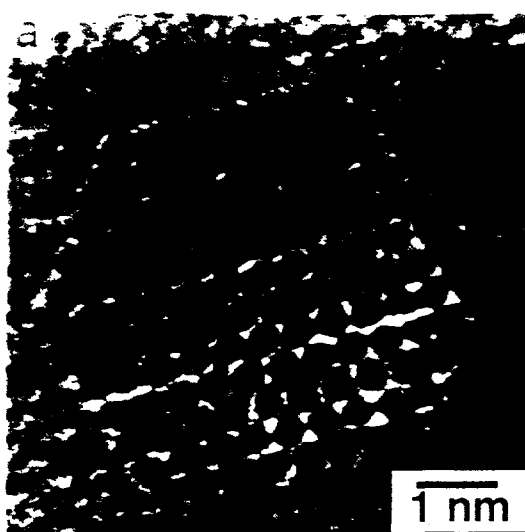


Figure 4.

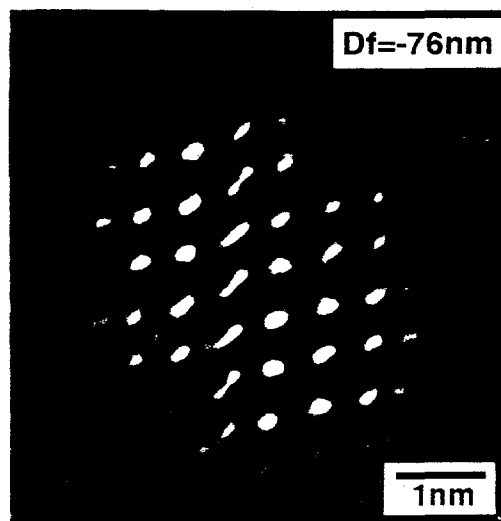


Figure 5.

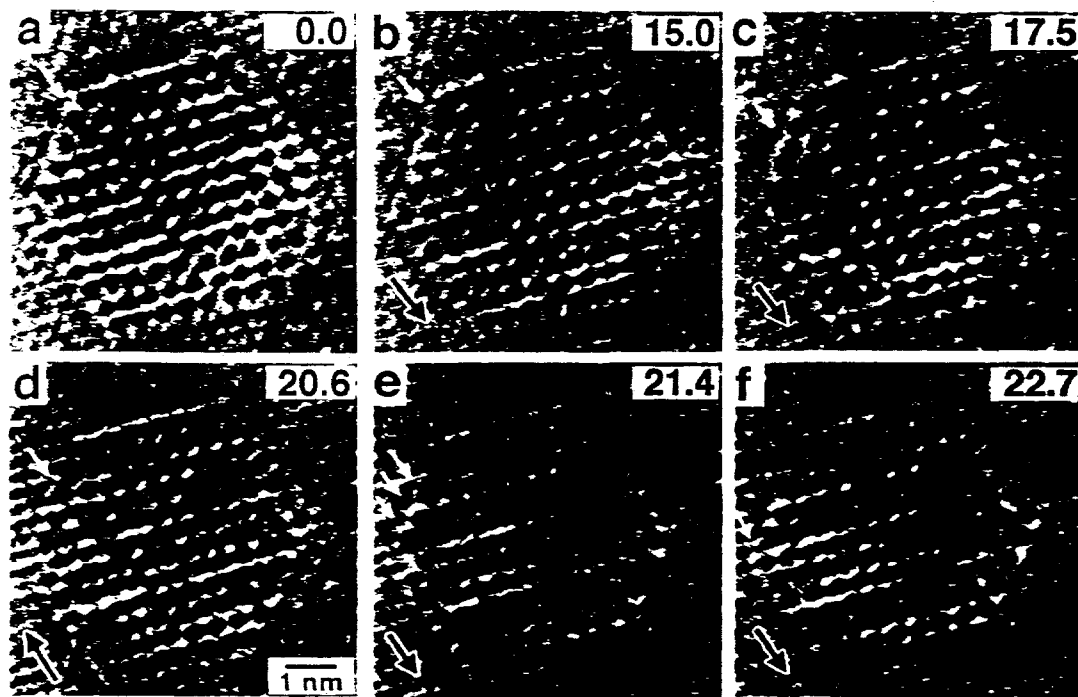


Figure 6.